JOURNAL OF MOLECULAR SPECTROSCOPY **176,** 268–273 (1996)
ARTICLE NO. 0086

High-Resolution Laser Excitation Spectroscopy of the $\tilde{B}^2\Sigma^+$–$\tilde{X}^2\Sigma^+$ System of Jet-Cooled SrOD

C. Zhao, P. G. Hajigeorgiou, P. F. Bernath, and J. W. Hepburn

Department of Chemistry, University of Waterloo, Waterloo, Ontario, Canada N2L 3G1

Received September 12, 1995

The high-resolution laser excitation spectrum of the 001–000 and 000–000 bands of the $\tilde{B}^2\Sigma^+$–$\tilde{X}^2\Sigma^+$ transition of SrOD was recorded. The SrOD molecules were made by pulsed laser ablation of Sr metal followed by reaction with D_2O. Sub-Doppler resolution and rotational cooling were achieved by expansion into vacuum and excitation with a cw dye laser perpendicular to the molecular beam. A molecular linewidth of 200 MHz and the lack of spectral congestion allowed a *Q* branch to be detected. Spin–orbit mixing between the $\tilde{A}^2\Pi$ and $\tilde{B}^2\Sigma^+$ states caused the unusual appearance of a moderate intensity *Q* branch in a nominally parallel $^2\Sigma^+$–$^2\Sigma^+$ transition. From the relative intensities of the rotational lines, the ratio of the perpendicular to the parallel transition dipole moment was found to be 0.2 to 0.3.

I. INTRODUCTION

In recent years, there has been a surge of interest in the alkaline earth monohydroxide molecules. For SrOH and SrOD, the pioneering work was the rotational analysis of the 000–000, 001–001, and 010–010 bands of the $\tilde{B}^2\Sigma^+$–$\tilde{X}^2\Sigma^+$ transition by Nakagawa *et al.* in 1983 (*1*). Since then, the 000–000 band of the $\tilde{A}^2\Pi$–$\tilde{X}^2\Sigma^+$ transition of SrOH has been analyzed (*2*), followed by work on additional bands of the $\tilde{A}$–$\tilde{X}$ (*3*) and $\tilde{B}$–$\tilde{X}$ (*4*) transitions. Microwave (*5*) and millimeter-wave (*6, 7*) spectra of SrOH are available and the dipole moments in the $\tilde{X}$, $\tilde{A}$, and $\tilde{B}$ states were determined from the Stark effect in a molecular beam (*8*). Semiempirical calculations based on a modified Rittner model (*9*) and ligand field theory (*10*) have been used to predict energy levels and dipole moments.

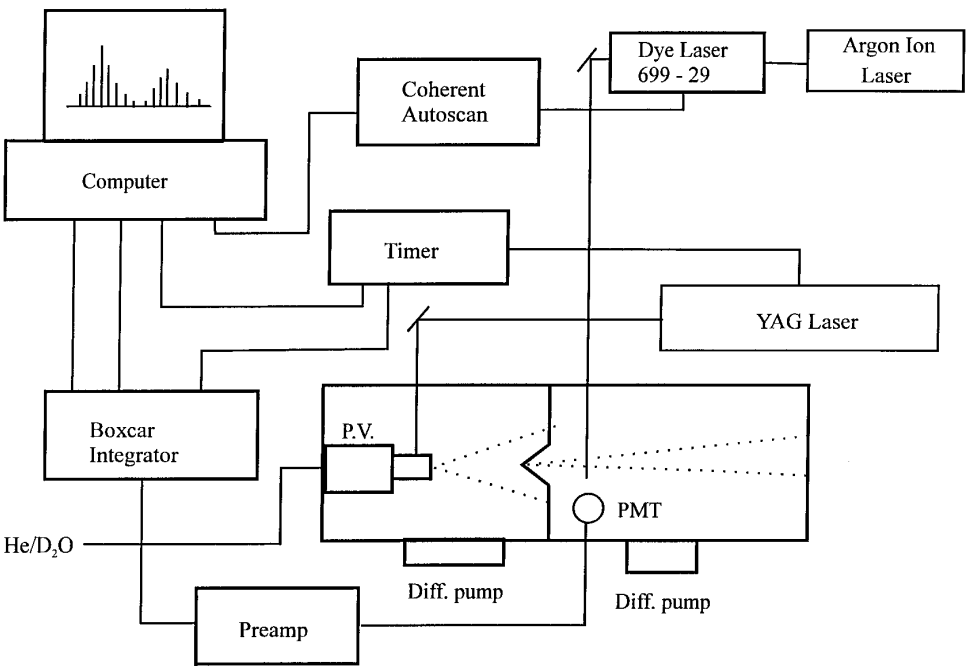

FIG. 1. A block diagram of the experimental apparatus.

0022-2852/96 $18.00

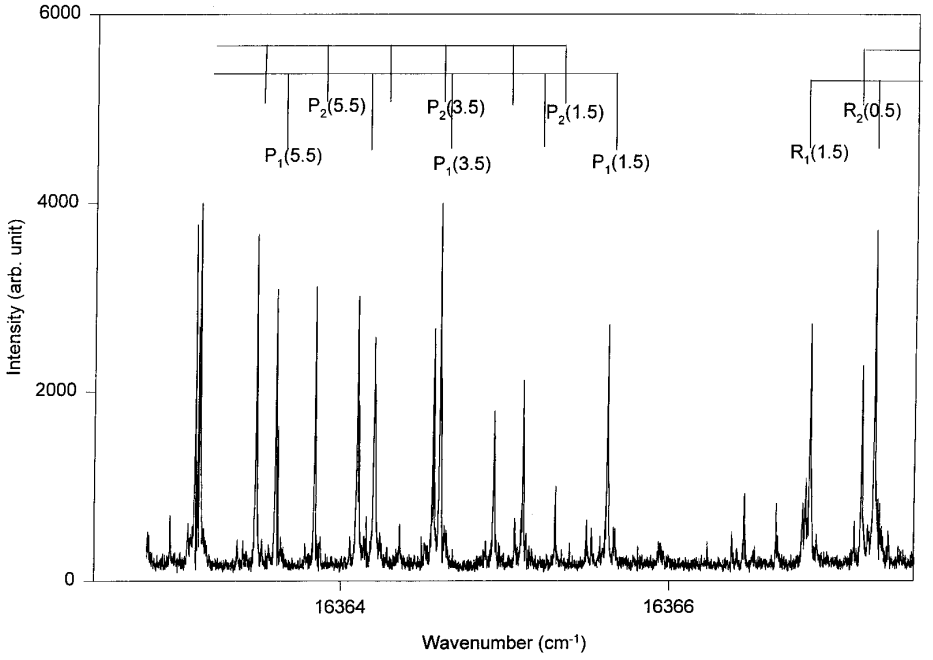

FIG. 2. A portion of the high-resolution spectrum showing *P* and *R* branches of the 000–000 band of the $\tilde{B}^2\Sigma^+ - \tilde{X}^2\Sigma^+$ transition of SrOD.

The previous spectrum of SrOD was recorded in a Broida oven (*1*) so that the resolution was limited by Doppler broadening and weak *Q*-branch lines were not seen. In a supersonic jet expansion, the molecules are vibrationally and rotationally cooled in order to simplify the spectrum. The molecular beam is crossed at right angles with a laser beam so that sub-Doppler spectra are obtained.

The 000–000 and 001–000 bands of the $\tilde{B}^2\Sigma^+ - \tilde{X}^2\Sigma^+$ system of SrOD were studied in our work. The $\tilde{A}^2\Pi_{1/2}$ and $\tilde{B}^2\Sigma^+$ states are mixed by off-diagonal spin–orbit coupling. The $\tilde{B}^2\Sigma^+ - \tilde{X}^2\Sigma^+$ is nominally a parallel transition which should have very weak *Q* branches which decrease rapidly in intensity as *J* increases. However, the $\tilde{A}^2\Pi_{1/2} \sim \tilde{B}^2\Sigma^+$ mixing induces some perpendicular character in the $\tilde{B}-\tilde{X}$ transition

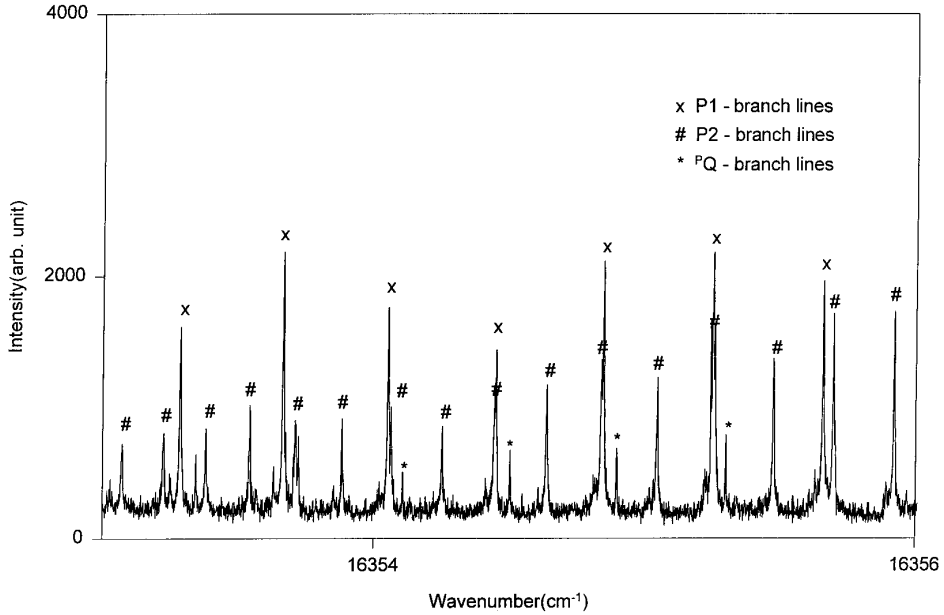

FIG. 3. The portion of the *P* branch of the 000–000 band of the $\tilde{B}^2\Sigma^+ - \tilde{X}^2\Sigma^+$ transition of SrOD showing *Q*-branch lines.

TABLE 1

Line Positions (in cm^{-1}) for the $\tilde{B}^2\Sigma^+(000)-\tilde{X}^2\Sigma^+(000)$ Band of SrOD

N	P1		N	P1		N	P1	
2	16365.6515	0.0049	9	16369.7975	-0.0063	43	16354.4190	-0.0067
3	16365.1368	0.0012	10	16370.2804	0.0383	44	16354.2740	0.0001
4	16364.6325	0.0025	11	16370.6845	-0.0010	45	16354.1237	-0.0038
5	16364.1319	0.0022	12	16371.1310	-0.0034	46	16353.9873	0.0007
6	16363.6358	0.0011	13	16371.5808	-0.0077	47	16353.8500	-0.0011
7	16363.1454	0.0002	14	16372.0461	-0.0018	48	16353.7222	0.0010
8	16362.6730	0.0120	15	16372.5094	-0.0033	49	16353.5959	-0.0007
9	16362.1860	0.0038	16	16372.9814	-0.0013	50	16353.4793	0.0017
10	16361.7160	0.0072	17	16373.4537	-0.0043	N	R2	
11	16361.2490	0.0082	18	16373.9390	0.0004	1	16367.2098	-0.0019
12	16360.7807	0.0025	19	16374.4237	-0.0006	2	16367.7458	0.0016
13	16360.3263	0.0054	20	16374.9158	0.0003	3	16368.2786	-0.0032
14	16359.8694	0.0003	21	16375.4129	0.0010	4	16368.8216	-0.0033
15	16359.4225	-0.0000	22	16375.9137	0.0002	5	16369.3697	-0.0036
16	16358.9821	0.0005	23	16376.4195	-0.0007	6	16369.9241	-0.0030
17	16358.5450	-0.0008	24	16376.9314	-0.0009	7	16370.4832	-0.0030
18	16358.1183	0.0026	N	P2		8	16371.0474	-0.0031
19	16357.7631	0.0722	2	16365.3374	0.0024	9	16371.6139	-0.0063
20	16357.2724	0.0009	3	16364.9629	0.0021	10	16372.1926	-0.0026
21	16356.8597	0.0022	4	16364.5934	0.0014	11	16372.7728	-0.0028
22	16356.4514	0.0025	5	16364.2346	0.0060	12	16373.3592	-0.0020
23	16356.0460	0.0003	6	16363.8732	0.0027	13	16373.9506	-0.0015
24	16355.6511	0.0031	7	16363.5160	-0.0017	14	16374.5508	0.0025
25	16355.2554	-0.0006	8	16363.1736	0.0031	15	16375.1461	-0.0036
26	16354.8695	0.0007	9	16362.8390	0.0105	16	16375.7562	-0.0003
27	16354.4889	0.0015	10	16362.5110	0.0190	17	16376.3689	0.0003
28	16354.1127	0.0013	11	16362.1860	0.0252	18	16376.9853	-0.0005
29	16353.7405	-0.0002	12	16361.8380	0.0030	N	Q1ef	
30	16353.3757	0.0000	13	16361.5230	0.0083	12	16360.3522	0.0038
31	16353.0151	-0.0008	14	16361.1990	-0.0006	13	16359.9025	0.0037
32	16352.6616	-0.0001	15	16360.9060	0.0159	14	16359.4536	-0.0008
33	16352.3105	-0.0024	16	16360.5886	0.0027	15	16359.0171	0.0014
34	16351.9696	0.0000	17	16360.2904	0.0032	16	16358.5822	0.0000
35	16351.6309	-0.0007	18	16359.9958	0.0020	17	16358.1572	0.0030
36	16351.2959	-0.0032	19	16359.7084	0.0025	18	16357.7332	0.0016
37	16350.9717	-0.0004	20	16359.4225	-0.0008	20	16356.8977	-0.0048
38	16350.6488	-0.0018	21	16359.1490	0.0028	21	16356.4990	0.0028
39	16350.3352	0.0006	22	16358.8720	-0.0025	22	16356.0958	0.0006
40	16350.0248	0.0009	23	16358.6072	-0.0010	23	16355.7032	0.0035
41	16349.7189	0.0001	24	16358.3487	0.0012	24	16355.3101	0.0005
42	16349.4194	0.0004	25	16358.0881	-0.0039	25	16354.9256	0.0007
43	16349.1239	-0.0008	26	16357.8424	0.0003	26	16354.5472	0.0015
44	16348.8379	0.0019	27	16357.6000	0.0024	27	16354.1728	0.0009
45	16348.5538	0.0011	28	16357.3595	0.0010	28	16353.8020	-0.0015
46	16348.2736	-0.0011	29	16357.1239	-0.0008	29	16353.4401	-0.0004
47	16348.0040	0.0016	30	16356.8976	0.0010	30	16353.0827	-0.0003
48	16347.7337	-0.0017	31	16356.6756	0.0017	31	16352.7305	-0.0005
49	16347.4732	-0.0007	32	16356.4513	-0.0051	32	16352.3793	-0.0051
50	16347.2210	0.0030	33	16356.2453	0.0007	33	16352.0425	-0.0007
N	R1		34	16356.0459	0.0077	N	Q1fe	
2	16366.8911	0.0058	35	16355.8376	0.0004	11	16372.1704	-0.0017
3	16367.2867	0.0005	36	16355.6510	0.0093	12	16372.7496	-0.0007
4	16367.6962	0.0037	37	16355.4537	0.0021	13	16373.3324	-0.0013
5	16368.0986	-0.0054	38	16355.2655	-0.0014	14	16373.8896	-0.0328
6	16368.5166	-0.0044	39	16355.0861	-0.0017	15	16374.5189	0.0025
7	16368.9412	-0.0021	40	16354.9255	0.0114	16	16375.1119	-0.0037
8	16369.3697	-0.0012	41	16354.7461	0.0002	17	16375.7193	-0.0009
			42	16354.5834	0.0003			

Note. The table shows ν_{obs} and the residuals, $\nu_{obs} - \nu_{calc}$.

TABLE 2

Line Positions (in cm^{-1}) for the $\tilde{B}^2\Sigma^+(001) - \tilde{X}^2\Sigma^+(000)$ Band of SrOD

N	P1		N	P1		N	P1	
2	16889.3002	0.0014	17	16896.7066	-0.0005	26	16880.6474	0.0016
3	16888.7894	0.0044	18	16897.1420	0.0015	27	16880.3359	0.0026
4	16888.2777	0.0037	19	16897.5773	0.0009	28	16880.0243	0.0007
5	16887.7692	0.0034	20	16898.0116	-0.0033	29	16879.7163	-0.0004
6	16887.2662	0.0060	21	16898.4574	0.0012	30	16879.4122	-0.0005
7	16886.7579	0.0005	22	16898.9022	0.0022	31	16879.1117	0.0001
8	16886.2566	-0.0007	23	16899.3456	-0.0008	32	16878.8141	0.0009
9	16885.7600	0.0000	24	16899.7956	0.0000	33	16878.5174	-0.0002
10	16885.2648	-0.0008	25	16900.2476	0.0003	34	16878.2188	-0.0061
11	16884.7716	-0.0022	26	16900.7009	-0.0007	35	16877.9318	-0.0033
12	16884.2860	0.0010	27	16901.1586	0.0000	36	16877.6482	0.0000
13	16883.8036	0.0048	28	16901.6203	0.0021	37	16877.3591	-0.0048
14	16883.3195	0.0042	29	16902.0793	-0.0012	38	16877.0800	-0.0026
15	16882.8349	0.0002	30	16902.5450	0.0000	41	16876.2504	-0.0054
16	16882.3551	-0.0016	31	16903.0139	0.0014	42	16875.9775	-0.0084
17	16881.8814	-0.0003	32	16903.4854	0.0030			
18	16881.4109	0.0014	33	16903.9499	-0.0049	N	R2	
19	16880.9395	-0.0004	34	16904.4309	0.0009	1	16890.8550	-0.0014
20	16880.4732	-0.0000	35	16904.9109	0.0033	2	16891.3769	-0.0041
21	16880.0088	-0.0005	36	16905.389	0.0011	3	16891.9081	-0.0003
22	16879.5479	-0.0003	37	16905.8718	0.0012	4	16892.4387	0.0001
23	16879.0891	-0.0008	38	16906.3546	-0.0013	5	16892.9694	-0.0019
24	16878.6323	-0.0021	39	16906.8453	0.0015	6	16893.5045	-0.0024
25	16878.1792	-0.0025	40	16907.335	0.0007	7	16894.0394	-0.0057
26	16877.7286	-0.0033	41	16907.8275	0.0003	8	16894.5799	-0.0061
27	16877.2818	-0.0031	42	16908.3238	0.0011	9	16895.1272	-0.0024
28	16876.8380	-0.0026	43	16908.823	0.0023	10	16895.6681	-0.0078
29	16876.3982	-0.0011	44	16909.3218	0.0006	11	16896.2109	-0.0014
30	16875.9611	0.0003	45	16909.8225	-0.0016	12	16896.7550	-0.0215
31	16875.5238	-0.0011	46	16910.3286	-0.0011	13	16897.2680	-0.0628
32	16875.0904	-0.0016	47	16910.8386	0.0008	14	16897.9202	0.0323
33	16874.6626	0.0006	48	16911.3494	0.0011	15	16898.4574	0.0098
34	16874.2339	-0.0009				16	16899.0203	0.0104
35	16873.8129	0.0025	N	P2		17	16899.5835	0.0086
36	16873.3874	-0.0014	2	16888.9835	-0.0012	18	16900.1508	0.0082
37	16872.9705	0.0004	3	16888.6067	0.0012	19	16900.7045	-0.0082
38	16872.5524	-0.0018	4	16888.2286	-0.0003	20	16901.2899	0.0041
39	16872.1389	-0.0022	5	16887.8517	-0.0034	21	16901.8658	0.0045
40	16871.7306	-0.0004	6	16887.4815	-0.0025	22	16902.4432	0.0037
41	16871.3221	-0.0015	7	16887.1089	-0.0068	23	16903.0156	-0.0046
			8	16886.7473	-0.0028	24	16903.6055	0.0017
N	R1		9	16886.383	-0.0043	25	16904.1925	0.0027
1	16890.1375	-0.0015	10	16886.0206	-0.0067	26	16904.7808	0.0023
2	16890.5298	0.0004	11	16885.6632	-0.0069	27	16905.3890	0.0192
4	16891.3161	-0.0018	12	16885.3084	-0.0072	28	16905.9636	0.0000
5	16891.7142	-0.0021	13	16884.9590	-0.0049	29	16906.5614	0.0013
6	16892.1161	-0.0013	14	16884.5930	-0.0219	30	16907.1614	0.0022
7	16892.5228	0.0015	15	16884.2052	-0.0636	31	16907.7611	0.0003
8	16892.9267	-0.0010	16	16883.9574	0.0319	32	16908.3238	-0.0412
9	16893.3393	0.0023	17	16883.6001	0.0152	33	16908.9715	-0.0003
10	16893.7518	0.0029	18	16883.2610	0.0138	34	16909.5806	-0.0005
11	16894.1647	0.0012	19	16882.9201	0.0079	35	16910.2017	0.0086
12	16894.5799	-0.0008	20	16882.5891	0.0091	36	16910.8073	-0.0002
13	16895.0033	0.0026	21	16882.2558	0.0052	37	16911.4256	0.0009
14	16895.4258	0.0025	22	16881.9275	0.0035	38	16912.0424	-0.0018
15	16895.8499	0.0013	23	16881.6035	0.0032	39	16912.6662	-0.0001
16	16896.2756	-0.0009	24	16881.2805	0.0012	41	16913.9366	0.0183
			25	16880.9627	0.0015	42	16914.5526	0.0046

Note. The table shows ν_{obs} and the residuals, $\nu_{obs} - \nu_{calc}$.

TABLE 3
Molecular Constants for SrOD (in cm^{-1})

Constant	$\tilde{X}\,^2\Sigma^+(000)$	$\tilde{B}\,^2\Sigma^+(000)$	$\tilde{B}\,^2\Sigma^+(001)$
B	0.22531615(82)	0.227992(24)	0.226681(45)
D	1.66514(89)E-7	1.6930(46)E-7	1.6833(72)E-7
γ	0.00219960(17)	-0.129270(92)	-0.129510(32)
T_0	-	16366.0983(01)	16889.7505(08)

and enhances the intensity of the *Q* branches. By comparing the intensities of the *P*, *Q*, and *R* branches, it is possible to deduce the ratio of the parallel to the perpendicular transition dipole moment.

With the exception of the millimeter-wave work (*6*) on SrOD, all of the recent studies have concentrated on SrOH. We report here on the analysis of the 001−000 and 000−000 bands of SrOD, recorded in order to test a new laser ablation spectrometer.

II. EXPERIMENTAL

The block diagram of the experimental apparatus is given in Fig. 1. The apparatus had two separately pumped chambers in order to produce a collimated supersonic beam. The ablation source chamber was pumped by a 10-in. diffusion pump (250/2000 Edwards), while the detection chamber was pumped by a 4-in. diffusion pump (100/300 Edwards). The supersonic molecular beam was produced by a homemade piezo-driven pulsed valve and collimated by a 3-mm-diameter stainless-steel skimmer located 3 cm from the nozzle (*5, 8*). The second harmonic (532 nm) of a 10 Hz pulsed Nd/YAG laser was used to vaporize the metal. The beam was formed by expansion of 2.7 atm (40 psi) of helium flowing over liquid D_2O. The stainless-steel nozzle can accept a metal sample rod with a diameter up to 8 mm. This rod was rotated and translated during the experiment. The ablation laser was weakly focused onto the sample and entered the sample holder through a 1-mm hole. The expansion channel was about 1 mm in diameter and 10 mm long.

The signal was detected by monitoring the laser-induced fluorescence (LIF) produced by the molecular beam when it intersected the probe laser beam from a cw-ring dye laser 12 cm downstream from the skimmer. A Hamamatsu photomultiplier tube (R943-02) was aligned perpendicular to both the molecular beam and the probe laser beam, and the LIF was collected through a lens assembly. A narrow bandpass filter (40 nm) centered at the laser frequency was used for the 000−000 transition. A bandpass filter (40 nm) centered on the 001−001 transition and a red-pass filter were used for 001−000 transition, and in this way a much better signal-to-noise ratio was obtained. The bandpass filter was very effective at eliminating most of the plasma radiation from the ablation source. A boxcar integrator was used to process the LIF signal. A time ''window'' of 20 μsec was opened after a 100 μsec delay from when the ablation laser fired. To increase the signal-to-noise ratio, the scan time of the ring dye laser was set such that at least five pulses were averaged for each frequency point. Therefore, 100 sec was needed for each 10 GHz scan using 50 MHz steps.

The Coherent Autoscan 699-29 dye ring laser was calibrated with the I_2 lines (*11*) recorded at the same time during the experiment. The absolute accuracy of the line positions is about 0.003 cm^{-1}.

III. RESULTS AND DISCUSSION

The analysis of the 001−000 and 000−000 bands of the $\tilde{B}^2\Sigma^+-\tilde{X}^2\Sigma^+$ transition of SrOD was straightforward with the help of the previous work (*1*). As a result of rotational cooling, the first few lines and the band origin were easily located (Fig. 2). The line positions of the two bands were measured with a program called Decomp and are reported in Tables 1 and 2.

The line positions were fitted using the standard N^2 Hamiltonian evaluated using Hund's case (*a*) basis functions (*12*). The 001−000 and 000−000 bands, and the pure rotational transitions (*6*) were fitted together to provide the constants of Table 3. A small perturbation was noted in the excited state F_2 component of the 001 $\tilde{B}^2\Sigma^+$ state close to $N' = 14$, $J' = 13.5$, f parity (Table 2). These lines were included with reduced weights in the final fit.

For pure $^2\Sigma^+-{}^2\Sigma^+$ transitions, *Q* branches are very weak in intensity. If there is $^2\Pi_{1/2}$ character mixed into a $^2\Sigma^+$ state, then the intensity of the *Q* branches is enhanced. Kopp and Hougen (*13*) considered the intensity of the branches of a general $\frac{1}{2}-\frac{1}{2}$ transition and derived the following formulas:

$$P_{ee}: \quad [(J + \tfrac{1}{2})(J - \tfrac{1}{2})/J][\mu_\parallel - \mu_\perp]^2$$

$$Q_{ef}: \quad [2(J + \tfrac{1}{2})^3/J(J + 1)][\mu_\parallel/(2J + 1) - \mu_\perp]^2.$$

Application of these expressions to the 000−000 band gives a ratio of $\mu_\perp/\mu_\parallel$ of about 0.2 to 0.3 for the $\tilde{B}^2\Sigma^+-\tilde{X}^2\Sigma^+$ transition of SrOD. The 001−000 band is weaker than the 000−000 band, so that *Q* branches were not detected. The value of the Sr−O stretching mode frequency, ν_3, in the $\tilde{B}^2\Sigma^+$ state of SrOD is found to be 523.652 cm^{-1} by subtraction of the band origins. The use of our 001−000 band origin and Nakagawa *et al.*'s (*1*) 001−001 band origin of 16 372.6281 gives a value of 517.122 cm^{-1} for ν_3 in the $\tilde{X}^2\Sigma^+$ state.

IV. CONCLUSION

Our high-resolution study of SrOD has provided improved molecular constants. This resulted from the cooling of SrOD

in a supersonic expansion and a sub-Doppler linewidth. *Q*-branch lines were observed for the first time, and the ratio of the perpendicular to the parallel transition dipole moment was estimated.

ACKNOWLEDGMENT

We thank the National Sciences and Engineering Research Council of Canada (NSERC) for support of this research.

REFERENCES

1. J. Nakagawa, R. F. Wormsbecher, and D. O. Harris, *J. Mol. Spectrosc.* **97,** 37–64 (1983).
2. C. R. Brazier and P. F. Bernath, *J. Mol. Spectrosc.* **114,** 163–173 (1985).
3. P. I. Presunka and J. A. Coxon, *J. Chem. Phys.* **101,** 201–222 (1994).
4. P. I. Presunka and J. A. Coxon, *Can. J. Chem.* **71,** 1689–1705 (1993).
5. D. A. Fletcher, K. Y. Jung, C. T. Scurlock, and T. C. Steimle, *J. Chem. Phys.* **98,** 1837–1842 (1993).
6. M. A. Anderson, W. L. Barclay, and L. M. Ziurys, *Chem. Phys. Lett.* **196,** 166–172 (1992).
7. D. A. Fletcher, M. A. Anderson, W. L. Barclay, and L. M. Ziurys, *J. Chem. Phys.* **102,** 4334–4339 (1995).
8. T. C. Steimle, D. A. Fletcher, K. Y. Jun, and C. T. Scurlock, *J. Chem. Phys.* **96,** 2556–2564 (1992).
9. J. M. Mestdagh and J. P. Visticot, *Chem. Phys.* **155,** 79–89 (1991).
10. A. R. Allouche and M. Aubert-Frécon, *J. Mol. Spectrosc.* **163,** 599–603 (1994).
11. S. Gerstenkorn and P. Luc, ''Atlas du Spectre d'Absorption de la Molécule d'Iode.'' Laboratoire Aimé-Cotton, CNRS II, 91405 Orsay, France, 1978.
12. M. Douay, S. A. Rogers, and P. F. Bernath, *Mol. Phys.* **64,** 425–436 (1988).
13. I. Kopp and J. T. Hougen, *Can. J. Phys.* **45,** 2581–2596 (1967).